

Numerical simulation of fluid-structure interaction with application to aneurysm hemodynamics

M. Razzaq, S. Turek, J. Hron, J. F. Acker, F. Weichert, M. Wagner, I. Q. Grunwald, C. Roth, and B. F. Romeike

As an example for fluid-structure interaction in biomedical problems, the influence of endovascular stent implantation onto cerebral aneurysm hemodynamics is numerically investigated. The aim is to study the interaction of the elastic walls of the aneurysm with the geometrical shape of the implanted stent structure for prototypical 2D configurations. This study can be seen as a basic step towards the understanding of the resulting complex flow phenomena so that in future aneurysm rupture shall be suppressed by an optimal setting for the implanted stent geometry. From the mathematical side, numerical techniques for solving the problem of fluid-structure interaction with an elastic material in a laminar incompressible viscous flow are described. An Arbitrary Lagrangian-Eulerian (ALE) formulation is employed in a fully coupled monolithic way, considering the problem as one continuum. The mathematical description and the numerical schemes are designed in such a way that more complicated constitutive relations (and more realistic for biomechanics applications) for the fluid as well as the structural part can be easily incorporated. We utilize the well-known Q_2P_1 finite element pair for discretization in space to gain high accuracy and perform as time-stepping the 2nd order Crank-Nicholson, resp., Fractional-Step- θ -scheme for both solid and fluid parts. The resulting nonlinear discretized algebraic system is solved by a Newton method which approximates the Jacobian matrices by the divided differences approach, and the resulting linear systems are solved by iterative solvers, preferably of Krylov-multigrid type. Preliminary results for the stent-assisted occlusion of cerebral aneurysm are presented. Since these results are currently restricted to 2D configurations, the aim is not to predict quantitatively the complex interaction mechanisms between stents and elastic walls of the aneurysm, but to analyse qualitatively the behaviour of the elasticity of the walls vs. the geometrical details of the stent for prototypical flow situations.

1 Introduction

In this contribution, we consider the general problem of viscous flow interacting with an elastic body which is being deformed by the fluid action. Such a problem is of great importance in many real life applications, and typical examples of this type of problem are the areas of biomedical fluids which include the influence of hemodynamic factors in blood vessels, cerebral aneurysm hemodynamics, joint lubrication and deformable cartilage and blood flow interaction with elastic veins (Appanaboyina et al., 2008), (Valencia et al., 2008), (Fernandez et al., 2008), (Tezduyar et al., 2007), (Tezduyar et al., 2008). The theoretical investigation of fluid-structure interaction problems is complicated by the need of a mixed description for both parts: While for the solid part the natural view is the material (Lagrangian) description, for the fluid it is usually the spatial (Eulerian) description. In the case of their combination some kind of mixed description (usually referred to as the Arbitrary Lagrangian-Eulerian description or ALE) has to be used which brings additional nonlinearity into the resulting equations (see (Hron and Turek, 2006b)).

The numerical solution of the resulting equations of the fluid-structure interaction problem poses great challenges since it includes the features of structural mechanics, fluid dynamics and their coupling. The most straightforward solution strategy, mostly used in the available software packages (see for instance (Hron et al., 2002)), is to decouple the problem into the fluid part and solid part, for each of those parts using some well established method of solution; then the interaction process is introduced as external boundary conditions in each of the subproblems. This has the advantage that there are many well tested numerical methods for both separate problems of fluid flow and elastic deformation, while on the other hand the treatment of the interface and the interaction is problematic due to high stiffness and sensitivity. In contrast, the monolithic approach discussed here treats the problem as a

single continuum with the coupling automatically taken care of as internal interface.

Beside a short description of the underlying numerical aspects regarding discretization and solution procedure for this monolithic approach (see (Razzaq et al., 2008), (Hron and Turek, 2006a)), we concentrate on prototypical numerical studies for 2D aneurysm configurations. The corresponding parametrization was based on abstractions of biomedical data (i.e., cutplanes of 3D specimens from New Zealand white rabbits as well as computer tomographic and magnetic resonance imaging data of human neurocrania). In our studies, we allow the walls of the aneurysm to be elastic and hence deforming with the flow field in the vessel. Moreover, we examine several configurations for stent geometries which clearly influence the flow behavior inside of the aneurysm such that a very different elastic displacement of the walls is observed too. We demonstrate that either the elastic modeling of the aneurysm walls as well as the proper description of the geometrical details of the shape of the aneurysm and particularly of the stents is of great importance if the complex interaction between structure and fluid shall be quantitatively analyzed in future, especially in view of more realistic blood flow models and anisotropic constitutive laws of the elastic walls.

2 Fluid-structure interaction problem formulation

The general fluid-structure interaction problem consists of the description of the fluid and solid fields, appropriate interface conditions at the interface and conditions for the remaining boundaries, respectively. In this paper, we consider the flow of an incompressible Newtonian fluid interacting with an elastic solid. We denote the domain occupied by the fluid by Ω_t^b and the solid by Ω_t^s at the time $t \in [0, T]$. Let $\Gamma_t^0 = \bar{\Omega}_t^b \cap \bar{\Omega}_t^s$ be the part of the boundary where the elastic solid interacts with the fluid. In the following, the description for both fields and the interface conditions are introduced. Furthermore, discretization aspects and solution procedures are presented in the next section.

2.1 Constitutive relations for the fluid

The fluid is considered to be **Newtonian, incompressible** and its state is described by the *velocity* and *pressure* fields \mathbf{v}^b , p^b respectively. The constant density of the fluid is ρ^b and the kinematic viscosity is denoted by ν^b . The balance equations are:

$$\rho^b \frac{D\mathbf{v}^b}{Dt} = \operatorname{div} \boldsymbol{\sigma}^b, \quad \operatorname{div} \mathbf{v}^b = 0 \quad \text{in } \Omega_t^b \quad (1)$$

In order to solve the balance equations we need to specify the constitutive relations for the stress tensors. For the fluid we use the incompressible Newtonian relation

$$\boldsymbol{\sigma}^b = -p^b \mathbf{I} + \mu (\nabla \mathbf{v}^b + (\nabla \mathbf{v}^b)^T), \quad (2)$$

where μ represents the dynamic viscosity of the fluid and p^b is the Lagrange multiplier corresponding to the incompressibility constraint in (1). The material time derivative depends on the choice of the reference system. There are basically 3 alternative reference systems: the Eulerian, the Lagrangian, and the Arbitrary Lagrangian-Eulerian formulation. The most commonly used description for the fluid-structure interaction is the ALE description. For the ALE formulation presented in this paper, corresponding discretization techniques are discussed in section 3. Let us remark that also nonnewtonian flow models can be used for modeling blood flow, for instance of Power Law type or even including viscoelastic effects (see (Damanik et al., 2008)) which is planned for future extensions.

2.2 Constitutive relations for the structure

The structure is assumed to be **elastic** and **compressible**. Its configuration is described by the displacement \mathbf{u}^s , with velocity field $\mathbf{v}^s = \frac{\partial \mathbf{u}^s}{\partial t}$. The balance equations are:

$$\rho^s \frac{\partial \mathbf{v}^s}{\partial t} + \rho^s (\nabla \mathbf{v}^s) \mathbf{v}^s = \operatorname{div} \boldsymbol{\sigma}^s + \rho^s \mathbf{g}, \quad \text{in } \Omega_t^s. \quad (3)$$

Written in the more common Lagrangian description, i.e. with respect to some fixed reference (initial) state Ω^s , we have

$$\rho^s \frac{\partial^2 \mathbf{u}^s}{\partial t^2} = \operatorname{div} (J \boldsymbol{\sigma}^s \mathbf{F}^{-T}) + \rho^s \mathbf{g}, \quad \text{in } \Omega^s. \quad (4)$$

The constitutive relations for the stress tensors for the compressible structure are presented, however, also incompressible structures can be handled in the same way (see (Hron and Turek, 2006b)). The density of the structure in the undeformed configuration is ρ^s . The material elasticity is characterized by a set of two parameters, the Poisson ratio ν^s and the Young modulus E . Alternatively, the characterization is described by the Lamé coefficients λ^s and the shear modulus μ^s . These parameters satisfy the following relations

$$\nu^s = \frac{\lambda^s}{2(\lambda^s + \mu^s)} \quad E = \frac{\mu^s(3\lambda^s + 2\mu^s)}{(\lambda^s + \mu^s)} \quad (5)$$

$$\mu^s = \frac{E}{2(1 + \nu^s)} \quad \lambda^s = \frac{\nu^s E}{(1 + \nu^s)(1 - 2\nu^s)}, \quad (6)$$

where $\nu^s = 1/2$ for an incompressible and $\nu^s < 1/2$ for a compressible structure. In the large deformation case it is common to describe the constitutive equation using a stress-strain relation based on the Green Lagrangian strain tensor E and the 2.Piola-Kirchhoff stress tensor $S(E)$ as a function of E . The 2.Piola-Kirchhoff stress can be obtained from the Cauchy stress σ^s as

$$\mathbf{S}^s = J\mathbf{F}^{-1}\sigma^s\mathbf{F}^{-T}, \quad (7)$$

and the Green-Lagrange tensor E as

$$E = \frac{1}{2}(\mathbf{F}^T\mathbf{F} - I). \quad (8)$$

In this paper, the material is specified by giving the Cauchy stress tensor σ^s by the following constitutive law for the St.Venant-Kirchhoff material for simplicity

$$\sigma^s = \frac{1}{J}\mathbf{F}(\lambda^s(trE)I + 2\mu^s E)\mathbf{F}^T \quad \mathbf{S}^s = \lambda^s(trE)I + 2\mu^s E. \quad (9)$$

J denotes the determinant of the deformation gradient tensor \mathbf{F} , defined as $\mathbf{F} = I + \nabla\mathbf{u}^s$. Similar as in the case of more complex blood flow models, also more realistic constitutive relations for the anisotropic behavior of the walls of aneurysms can be included which however is beyond the scope of this contribution.

2.3 Interaction conditions

The boundary conditions on the fluid-solid interface are assumed to be

$$\sigma^b n = \sigma^s n, \quad \mathbf{v}^b = \mathbf{v}^s, \quad \text{on } \Gamma_t^0, \quad (10)$$

where n is a unit normal vector to the interface Γ_t^0 . This implies the no-slip condition for the flow and that the forces on the interface are in balance.

3 Discretization and solution techniques

In this study, we restrict at the moment to two dimensions which allows systematic tests of the proposed methods for biomedical applications in a very efficient way such that the qualitative behaviour can be carefully analyzed. The corresponding fully implicit, monolithic treatment of the fluid-structure interaction problem suggests that an A-stable second order time stepping scheme and that the same finite elements for both the solid part and the fluid region should be utilized. Moreover, to circumvent the fluid incompressibility constraints, we have to choose a stable finite element pair. For that reason, the conforming biquadratic, discontinuous linear Q_2P_1 pair, see Figure 1 for the location of the degrees of freedom, is chosen which will be explained in the next section.

3.1 Space discretization

Let us define the usual finite dimensional spaces U for displacement, V for velocity, P for pressure approximation as follows

$$\begin{aligned} U &= \{\mathbf{u} \in L^\infty(I, [W^{1,2}(\Omega)]^2), \mathbf{u} = \mathbf{0} \text{ on } \partial\Omega\}, \\ V &= \{\mathbf{v} \in L^2(I, [W^{1,2}(\Omega_t)]^2) \cap L^\infty(I, [L^2(\Omega_t)]^2), \mathbf{v} = \mathbf{0} \text{ on } \partial\Omega\}, \\ P &= \{p \in L^2(I, L^2(\Omega))\}, \end{aligned}$$

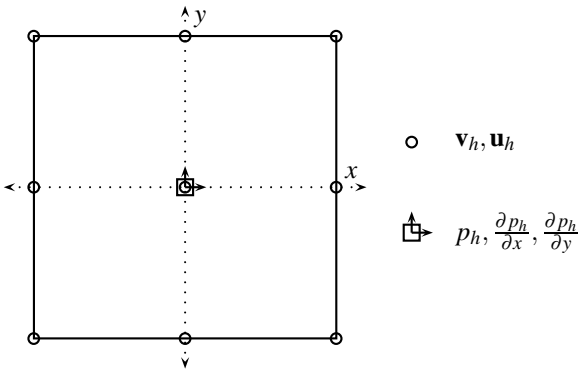


Figure 1: Location of the degrees of freedom for the Q_2P_1 element.

then the variational formulation of the fluid-structure interaction problem is to find $(\mathbf{u}, \mathbf{v}, p) \in U \times V \times P$ such that the equations are satisfied for all $(\zeta, \xi, \gamma) \in U \times V \times P$ including appropriate initial conditions. The spaces U, V, P on an interval $[t^n, t^{n+1}]$ would be approximated in the case of the Q_2, P_1 pair as

$$\begin{aligned} U_h &= \{\mathbf{u}_h \in [C(\Omega_h)]^2, \mathbf{u}_h|_T \in [Q_2(T)]^2 \quad \forall T \in \mathcal{T}_h, \mathbf{u}_h = \mathbf{0} \text{ on } \partial\Omega\}, \\ V_h &= \{\mathbf{v}_h \in [C(\Omega_h)]^2, \mathbf{v}_h|_T \in [Q_2(T)]^2 \quad \forall T \in \mathcal{T}_h, \mathbf{v}_h = \mathbf{0} \text{ on } \partial\Omega\}, \\ P_h &= \{p_h \in L^2(\Omega_h), p_h|_T \in P_1(T) \quad \forall T \in \mathcal{T}_h\}. \end{aligned}$$

Let us denote by \mathbf{u}_h^n the approximation of $\mathbf{u}(t^n)$, \mathbf{v}_h^n the approximation of $\mathbf{v}(t^n)$ and p_h^n the approximation of $p(t^n)$. Consider for each $T \in T_h$ the bilinear transformation $\psi_T : \hat{T} \rightarrow T$ to the unit square T . Then, $Q_2(T)$ is defined as

$$Q_2(T) = \{q \circ \psi_T^{-1} : q \in \text{span} \langle 1, x, y, xy, x^2, y^2, x^2y, y^2x, x^2y^2 \rangle\} \quad (11)$$

with nine local degrees of freedom located at the vertices, midpoints of the edges and in the center of the quadrilateral. The space $P_1(T)$ consists of linear functions defined by

$$P_1(T) = \{q \circ \psi_T^{-1} : q \in \text{span} \langle 1, x, y \rangle\} \quad (12)$$

with the function value and both partial derivatives located in the center of the quadrilateral, as its three local degrees of freedom, which leads to a discontinuous pressure. The inf-sup condition is satisfied (see (Boffi and Gastaldi, 2002)); however, the combination of the bilinear transformation ψ with a linear function on the reference square $P_1(\hat{T})$ would imply that the basis on the reference square did not contain the full basis. So, the method can at most be first order accurate on general meshes (see (Arnold et al., 2002), (Boffi and Gastaldi, 2002))

$$\|p - p_h\| = O(h). \quad (13)$$

The standard remedy is to consider a local coordinate system (ξ, η) obtained by joining the midpoints of the opposing faces of T (see (Arnold et al., 2002), (Rannacher and Turek, 1992), (Turek, 1999)). Then, we set on each element T

$$P_1(T) := \text{span} \langle 1, \xi, \eta \rangle. \quad (14)$$

For this case, the inf-sup condition is also satisfied and the second order approximation is recovered for the pressure as well as for the velocity gradient (see (Boffi and Gastaldi, 2002), (Gresho, 1990))

$$\|p - p_h\| = O(h^2) \quad \text{and} \quad \|\nabla(u - u_h)\|_0 = O(h^2). \quad (15)$$

For a smooth solution, the approximation error for the velocity in the L_2 -norm is of order $O(h^3)$ which can easily be demonstrated for prescribed polynomials or for smooth data on appropriate domains.

3.2 Time discretization

In view of a more compact presentation, the applied time discretization approach is described only for the fluid part (see (Razzaq, 2009) for more details). In the following, we restrict to the (standard) incompressible Navier-Stokes equations

$$\mathbf{v}_t - \nu \Delta \mathbf{v} + \mathbf{v} \cdot \nabla \mathbf{v} + \nabla p = \mathbf{f}, \quad \text{div } \mathbf{v} = 0, \quad \text{in } \Omega \times (0, T], \quad (16)$$

for given force \mathbf{f} and viscosity ν , with prescribed boundary values on the boundary $\partial\Omega$ and an initial condition at $t = 0$. Then, the usual θ -scheme for time discretization reads:

Basic θ -scheme: Given \mathbf{v}^n and $K = t_{n+1} - t_n$, then solve for $\mathbf{v} = \mathbf{v}^{n+1}$ and $p = p^{n+1}$

$$\frac{\mathbf{v} - \mathbf{v}^n}{K} + \theta[-\nu\Delta\mathbf{v} + \mathbf{v} \cdot \nabla\mathbf{v}] + \nabla p = \mathbf{g}^{n+1}, \quad \text{div } \mathbf{v} = 0, \quad \text{in } \Omega \quad (17)$$

with right hand side $\mathbf{g}^{n+1} := \theta\mathbf{f}^{n+1} + (1 - \theta)\mathbf{f}^n - (1 - \theta)[- \nu\Delta\mathbf{v}^n + \mathbf{v}^n \cdot \nabla\mathbf{v}^n]$.

The parameter θ has to be chosen depending on the time-stepping scheme, e.g., $\theta = 1$ for the Backward Euler (BE), or $\theta = 1/2$ for the Crank-Nicholson-scheme (CN) which we prefer. The pressure term $\nabla p = \nabla p^{n+1}$ may be replaced by $\theta\nabla p^{n+1} + (1 - \theta)\nabla p^n$, but with appropriate postprocessing, both strategies lead to solutions of the same accuracy. In all cases, we end up with the task of solving, at each time step, a nonlinear saddle point problem of given type which has then to be discretized in space as described above.

These two methods, CN and BE, belong to the group of *One-Step- θ -schemes*. The CN scheme can occasionally suffer from numerical instabilities because of its only weak damping property (not strongly A-stable), while the BE-scheme is of first order accuracy only (however: it is a good candidate for steady-state simulations). Another method which has proven to have the potential to excel in this competition is the *Fractional-Step- θ -scheme* (FS). It uses three different values for θ and for the time step K at each time level. In (Razzaq et al., 2008), (Turek et al., 2006) we additionally described a modified *Fractional-Step- θ -scheme* which particularly for fluid-structure interaction problems seems to be advantageous. A detailed description will appear in the thesis (Razzaq, 2009).

3.3 Solution algorithms

The system of nonlinear algebraic equations arising from the governing equations described above reads

$$\begin{bmatrix} S_{uu} & S_{uv} & 0 \\ S_{vu} & S_{vv} & kB \\ c_u B_s^T & c_v B_f^T & 0 \end{bmatrix} \begin{bmatrix} \mathbf{u} \\ \mathbf{v} \\ p \end{bmatrix} = \begin{bmatrix} \mathbf{f}_u \\ \mathbf{f}_v \\ f_p \end{bmatrix} \quad (18)$$

which is a typical saddle point problem, where S describes the diffusive and convective terms from the governing equations. The above system of nonlinear algebraic equations (18) is solved using Newton method as basic iteration. The basic idea of the Newton iteration is to find a root of a function, $\mathbf{R}(\mathbf{X}) = \mathbf{0}$, using the available known function value and its first derivative, where $\mathbf{X} = (\mathbf{u}_h, \mathbf{v}_h, p_h) \in U_h \times V_h \times P_h$. One step of the Newton iteration can be written as

$$\mathbf{X}^{n+1} = \mathbf{X}^n - \left[\frac{\partial \mathbf{R}}{\partial \mathbf{X}}(\mathbf{X}^n) \right]^{-1} \mathbf{R}(\mathbf{X}^n). \quad (19)$$

-
1. Let \mathbf{X}^n be some starting guess.
 2. Set the residuum vector $\mathbf{R}^n = \mathbf{R}(\mathbf{X}^n)$ and the tangent matrix $\mathbf{A} = \frac{\partial \mathbf{R}}{\partial \mathbf{X}}(\mathbf{X}^n)$.
 3. Solve for the correction $\delta\mathbf{X}$

$$\mathbf{A}\delta\mathbf{X} = \mathbf{R}^n.$$
 4. Find optimal step length ω .
 5. Update the solution $\mathbf{X}^{n+1} = \mathbf{X}^n - \omega\delta\mathbf{X}$.
-

Figure 2: One step of the Newton method with line search.

This basic iteration can exhibit quadratic convergence provided that the initial guess is sufficiently close to the solution. To ensure the convergence globally, some improvements of this basic iteration are used. The damped Newton method with line search improves the chance of convergence by adaptively changing the length of the correction vector. The solution update step in the Newton method (19) is replaced by

$$\mathbf{X}^{n+1} = \mathbf{X}^n - \omega\delta\mathbf{X}, \quad (20)$$

where the parameter ω is determined such that a certain error measure decreases (see (Turek, 1999), (Hron and Turek, 2006a) for more details). The Jacobian matrix $\frac{\partial \mathbf{R}(\mathbf{X}^n)}{\partial \mathbf{X}}$ can be computed by finite differences from the residual vector $\mathbf{R}(\mathbf{X})$

$$\left[\frac{\partial \mathbf{R}}{\partial \mathbf{X}} \right]_{ij} (\mathbf{X}^n) \approx \frac{[\mathbf{R}]_i(\mathbf{X}^n + \alpha_j \mathbf{e}_j) - [\mathbf{R}]_i(\mathbf{X}^n - \alpha_j \mathbf{e}_j)}{2\alpha_j}, \quad (21)$$

where \mathbf{e}_j are the unit basis vectors in \mathbb{R}^n and the coefficients α_j are adaptively taken according to the change in the solution in the previous time step. Since we know the sparsity pattern of the Jacobian matrix in advance, which is given by the used finite element method, this computation can be done in an efficient way so that the linear solver remains the dominant part in terms of the CPU time (see (Turek, 1999), (Turek and Schmachtel, 2002) for more details). A good candidate, at least in 2D, seems to be a direct solver for sparse systems like UMFPAK (see (Davis and Duff, 1999)); while this choice provides very robust linear solvers, its memory and CPU time requirements are too high for larger systems (i.e. more than 20.000 unknowns). Large linear problems can be solved by Krylov-space methods (BiCGStab, GMRes, see (Barrett et al., PA 1994)) with suitable preconditioners. One possibility is the ILU preconditioner with special treatment of the saddle point character of our system, where we allow certain fill-in for the zero diagonal blocks, see (Bramley and Wang, 1997).

As an alternative, we also utilize a standard geometric multigrid approach based on a hierarchy of grids obtained by successive regular refinement of a given coarse mesh. The complete multigrid iteration is performed in the standard defect-correction setup with the V or F-type cycle. While a direct sparse solver (Davis and Duff, 1999) is used for the coarse grid solution, on finer levels a fixed number (2 or 4) of iterations by local MPSC schemes (Vanka-like smoother) (Turek, 1999), (Vanka, 1985), (Hron and Turek, 2006a) is performed. Such iterations can be written as

$$\begin{bmatrix} \mathbf{u}^{l+1} \\ \mathbf{v}^{l+1} \\ p^{l+1} \end{bmatrix} = \begin{bmatrix} \mathbf{u}^l \\ \mathbf{v}^l \\ p^l \end{bmatrix} - \omega \sum_{\text{element} \Omega_i} \begin{bmatrix} S_{\mathbf{uu}}|_{\Omega_i} & S_{\mathbf{uv}}|_{\Omega_i} & 0 \\ S_{\mathbf{vu}}|_{\Omega_i} & S_{\mathbf{vv}}|_{\Omega_i} & kB|_{\Omega_i} \\ c_u B_s^T|_{\Omega_i} & c_v B_f^T|_{\Omega_i} & 0 \end{bmatrix}^{-1} \begin{bmatrix} \mathbf{def}_u^l \\ \mathbf{def}_v^l \\ def_p^l \end{bmatrix}.$$

The inverse of the local systems (39×39) can be done by hardware optimized direct solvers. The full nodal interpolation is used as the prolongation operator \mathbf{P} with its transposed operator used as the restriction $\mathbf{R} = \mathbf{P}^T$ (see (Hron et al., 2002), (Turek, 1999) for more details).

4 Problem description

In the following, we consider the numerical simulation of special problems encountered in the area of cardiovascular hemodynamics, namely flow interaction with thick-walled deformable material, which can become a useful tool for deeper understanding of the onset of diseases of the human circulatory system, as for example blood cell and intimal damages in stenosis, aneurysm rupture, evaluation of the new surgery techniques of heart, arteries and veins (see (Appanaboyina et al., 2008), (Löhner et al., 2008) (Valencia et al., 2008) and therein cited literature). In this contribution, prototypical studies are performed for brain aneurysm. The word ‘aneurysm’ comes from the latin word *aneurysma* which means dilatation. Aneurysm is a local dilatation in the wall of a blood vessel, usually an artery, due to a defect, disease or injury. Typically, as the aneurysm enlarges, the arterial wall becomes thinner and eventually leaks or ruptures, causing subarachnoid hemorrhage (SAH) (bleeding into brain fluid) or formation of a blood clot within the brain. In the case of a vessel rupture, there is a hemorrhage, and when an artery ruptures, then the hemorrhage is more rapid and more intense. In arteries the wall thickness can be up to 30% of the diameter and its local thickening can lead to the creation of an aneurysm so that the aim of numerical simulations is to relate the aneurysm state (unrupture or rupture) with wall pressure, wall deformation and effective wall stress. Such a relationship would provide information for the diagnosis and treatment of unrupture and rupture of an aneurysm by elucidating the risk of bleeding or rebleeding, respectively.

In order to use the proposed numerical methods for aneurysm hemodynamics, simplified two-dimensional examples, which however include the interaction of the flow with the deformable material, are considered. Flow through a deformable vein with elastic walls of a brain aneurysm is simulated to analyse qualitatively the described methods; here, the flow is driven by prescribing the flow velocity at the inflow part of the boundary while the elastic part of the boundary is either fixed or stress-free. Both ends of the walls are fixed at the inflow and outflow, and the flow is driven by a periodical change of the inflow at the left end.

4.1 Geometry of the problem

For convenience, the geometry of the fluid domain under consideration is currently based on 2D models (see Fig. 3) which allows us to concentrate on the detailed qualitative evaluation of our approach based on the described monolithic ALE formulation. The underlying construction of the (2D) shape of the aneurysm can be explained as follows:

- The bent blood vessel is approximated by quarter circles around the origin.
- The innermost circle has the radius $6mm$, the next has $8mm$, and the last one has $8.25mm$.
- This results in one rigid inner wall and an elastic wall between $8mm$ and $8.25mm$ of thickness $0.25mm$.

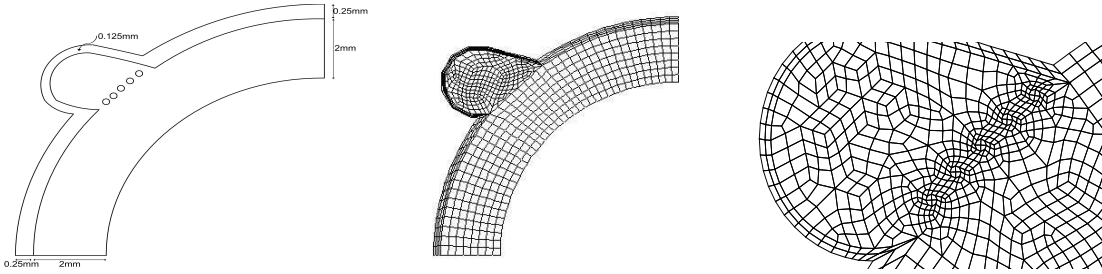


Figure 3: Left: Schematic drawing of the measurement section. Middle: Mesh without stents (776 elements). Right: Mesh with stents (1431 elements) which are part of the simulations.

The aneurysm shape is approximated by two arcs and lines intersecting the arcs tangentially. The midpoints of the arcs are the same $(-6.75; 6)$, they have the radius $1.125mm$ and $1.25mm$. They are intersected tangentially by lines at angular value 1.3 radians. This results in a wall thickness of $0.125mm$ for the elastic aneurysm walls (see Fig. 3). The examined stents are of circular shape, placed on the neck of the aneurysm, and we use three, resp., five stents (simplified ‘circles’ in 2D as cutplanes from 3D configurations) of different size and position. The stents also consist of a grid, immersed in the blood flow, which is located at the inlet of the aneurysm so that in future elastic deformations of the stents can be included, too, since in real life, the stent is a medical device which consists of a wire metal wire tube. Stents are typically used to keep arteries open and are located on the vessel wall while this stent is immersed in the blood flow (Fig. 3). The purpose of this device is to reduce the flux into and within the aneurysm in order to occlude it by a clot or rupture. The aneurysm is then intersected with the blood vessel and all missing angular values and intersection points can be determined.

4.2 Boundary and initial conditions

The (steady) velocity profile, to flow from the right to the left part of the channel, is defined as parabolic inflow, namely

$$\mathbf{v}^b(0, y) = \bar{U}(y - 6)(y - 8). \quad (22)$$

Correspondingly, the pulsatile inflow profile for the nonsteady tests for which peak systole and diastole occur for $\Delta t = 0.25s$ and $\Delta t = 0.75s$ respectively, is prescribed as

$$\mathbf{v}^b(t, 0, y) = \mathbf{v}^b(0, y)(1 + 0.75\sin(2\pi t)). \quad (23)$$

The natural outflow condition at the lower left part effectively prescribes some reference value for the pressure variable p , here $p = 0$. While this value could be arbitrarily set in the incompressible case, in the case of a compressible structure this might have influence onto the stress and consequently the deformation of the solid. The *no-slip* condition is prescribed for the fluid on the other boundary parts, i.e. top and bottom wall, stents and fluid-structure interface.

5 Numerical results

The newtonian fluid used in the tests has a density $\rho^b = 1.035 \times 10^{-6} \text{kg/mm}^3$ and a kinematic viscosity $\nu^b = 3.38 \text{mm}^2/\text{s}$ which is similar to the properties of blood. If we prescribe the inflow speed $\bar{U} = -50 \text{mm/s}$, this results in a Reynolds number $Re \approx 120$ based on the prescribed peak systole inflow velocity and the width of the veins which is 2mm such that the resulting flow is within the laminar region. Parameter values for the elastic vein in the described model are as follows: The density of the upper elastic wall is $\rho^s = 1.12 \times 10^{-6} \text{kg/mm}^3$, solid shear modulus is $\mu^s = 42.85 \text{kg/mms}^2$, Poisson ratio is $\nu^p = 0.4$, Young modulus is $E = 120 \text{kN/mm}^2$. As described before, the constitutive relations used for the materials are the incompressible Newtonian model (2) for the fluid and a hyperelastic neo-Hookean material for the solid. This choice includes most of the typical difficulties the numerical method has to deal with, namely the incompressibility and significant deformations.

From a medical point of view, the use of stents provides an efficient treatment for managing the difficult entity of intracranial aneurysms. Here, the thickness of the aneurysm wall is attenuated and the aneurysm hemodynamics changes significantly. Since the purpose of this device is to control the flux within the aneurysm in order to occlude it by a clot or rupture, the resulting flow behavior into and within the aneurysm is the main objective, particularly in view of the different stent geometries. Therefore, we decided for the 2D studies to locate the (2D parts of the) stents only in direct connection to the aneurysm.

Comparing our studies with the CFD literature (see (Fernandez et al., 2008), (Appanaboyina et al., 2008), (Valencia et al., 2008), (Torri et al., 2007a), (Torri et al., 2007b)), several research groups focus on CFD simulations with realistic 3D geometries, but typically assuming rigid walls. In contrast, we concentrate on the complex interaction between elastic deformations and flow perturbations induced by the stents. At the moment, we are only able to perform these simulations in 2D, however, with these studies we should be able to analyse qualitatively the influence of geometrical details onto the elastic material behavior, particularly in view of more complex blood models and constitutive equations for the structure. Therefore, the aims of our studies can be described as follows:

1. What is the influence of the elasticity of the walls onto the flow behavior inside of the aneurysm, particularly w.r.t. the resulting shape of the aneurysm?
2. What is the influence of the geometrical details of the (2D) stents, that means shape, size, position, onto the flow behavior into and inside of the aneurysm?
3. Do both aspects, small-scale geometrical details as well as elastic fluid-structure interaction, have to be considered simultaneously or is one of them negligible in first order approximation?
4. Are modern numerical methods and corresponding CFD simulations tools able to simulate qualitatively the multiphysics behavior of such biomedical configurations?

In the following, we show some corresponding results for the described prototypical aneurysm geometry, first for the steady state inflow profile, followed by nonsteady tests for the pulsatile inflow, both with rigid and elastic walls, respectively.

5.1 Steady configurations

Due to the given inflow profile, which is not time-dependent, and due to the low Re numbers, the flow behaviour leads to a steady state which only depends on the elasticity and the shape of the stents. Moreover, for the following simulations, we only treat the aneurysm wall as elastic structure. Then, the aneurysm undergoes some slight deformations which can hardly be seen in the following figures. However they result in a different volume of the flow domain (see Fig. 6) and lead to a significantly different local flow behaviour since the spacing between stents and elastic walls may change (see the subsequent color pictures).

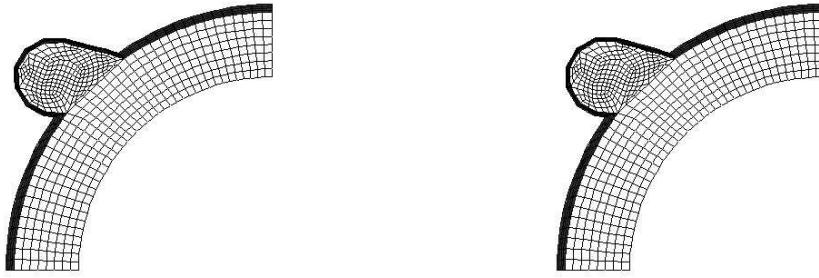


Figure 4: Deformed mesh for steady configuration without stents, with elastic wall (left). Mesh for rigid wall (right).



Figure 5: Deformed mesh for steady configuration with stents: 3 stents (left) and 5 stents (right).

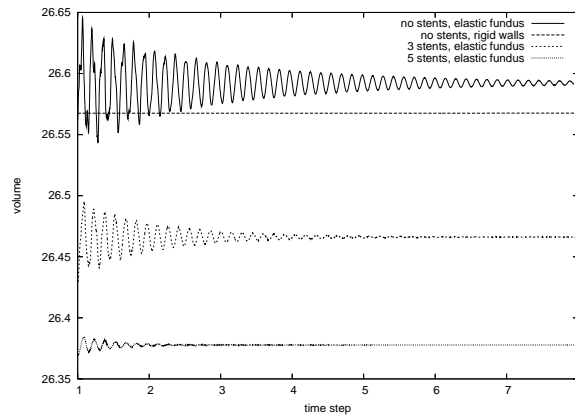


Figure 6: Resulting volume of the fluid domain for different configurations.

In the following pictures, we visualize the different flow behaviour by coloring due the velocity magnitude and by showing corresponding vector plots inside of the aneurysm. Particularly the influence of the number of stents onto the complete fluid flow through the channel including the aneurysm can be clearly seen.

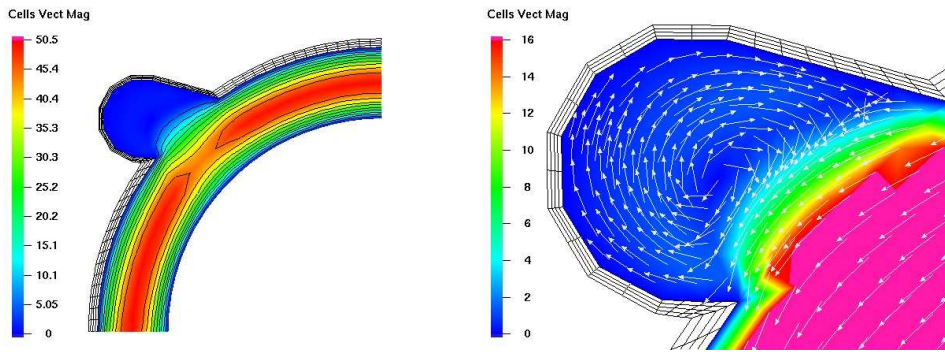


Figure 7: Rigid wall without stents.

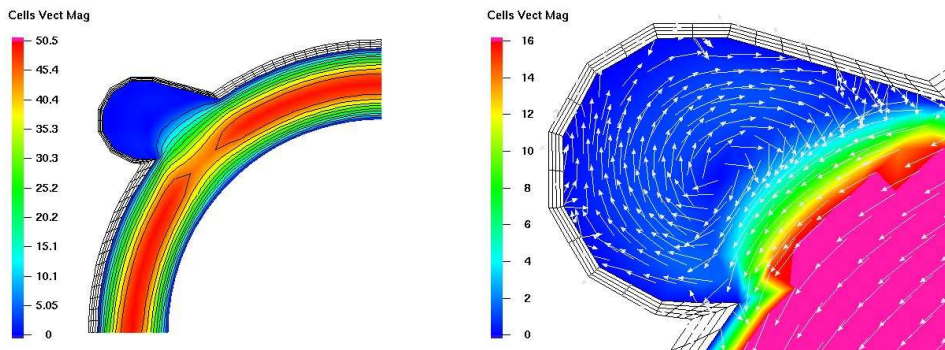


Figure 8: Elastic aneurysm wall without stents.

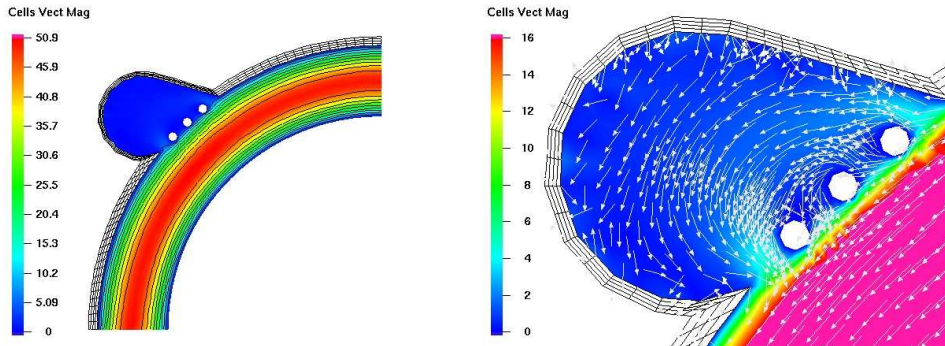


Figure 9: Elastic aneurysm wall with 3 stents.

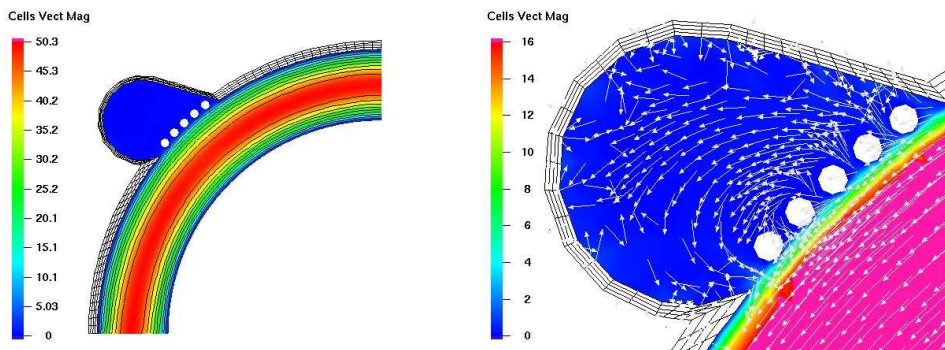


Figure 10: Elastic aneurysm wall with 5 stents.

Summarizing these results for steady inflow, the simulations show that the stent implantation across the neck of the aneurysm prevents blood penetration into the aneurysm fundus. Moreover, the elastic geometrical deformation of the wall is slightly reduced by implanting the stents while the local flow behaviour inside of the aneurysm is more significantly influenced by the elastic properties of the outer wall, particularly due to different width between stents and walls of the aneurysm. In the next section, we will consider the more realistic behaviour of flow configurations with time-dependent pulsatile inflow which will be analyzed for the case of elastic behaviour of the aneurysm walls.

5.2 Pulsatile configurations

For the following pulsatile test case, we have taken again the aneurysm part as elastic while the other parts of the walls belonging to the channel are rigid. First of all, we show again (see Fig. 11) the resulting volume of the flow domain for 5, 3 and no stents. In all cases, the oscillating behaviour due to the pulsatile inflow is visible which also leads to different volume sizes. Looking carefully at the resulting flow behaviour, we see global differences w.r.t. the channel flow near the aneurysm, namely due to the different flow rate into the aneurysm, and significant local differences inside of the aneurysm.

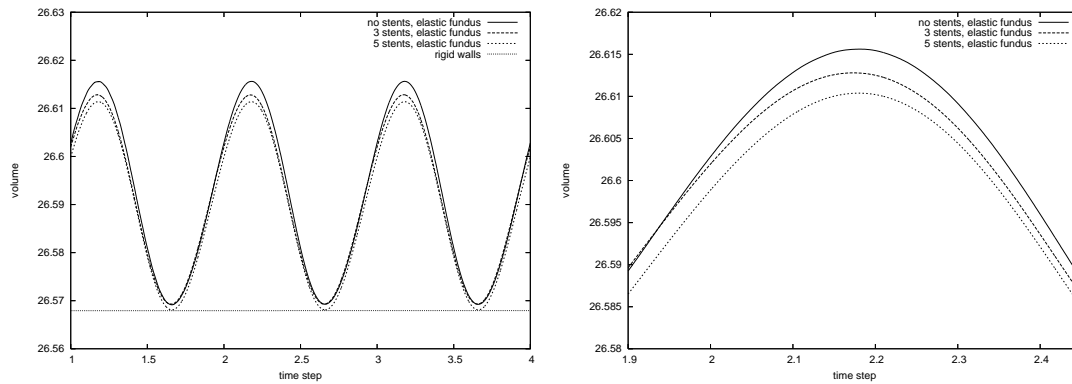


Figure 11: Volume of the domain with rigid and elastic behaviour of the aneurysm wall.

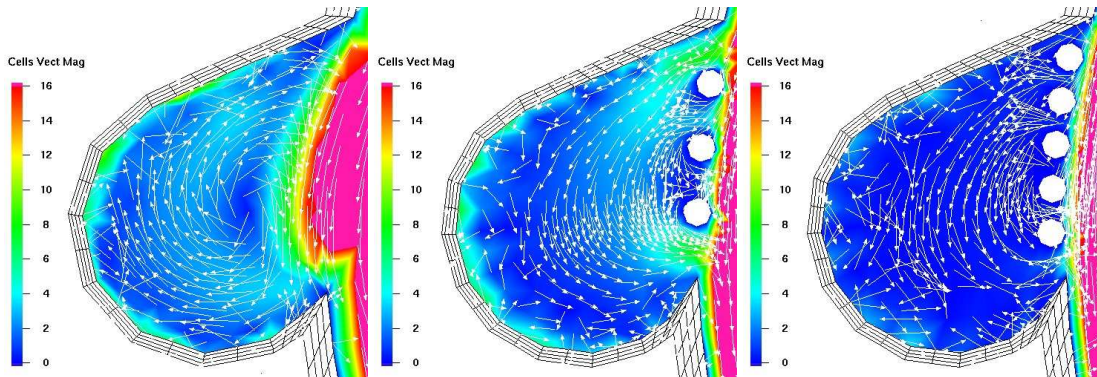


Figure 12: Snapshot for the magnitude of velocity for configurations with no, 3 and 5 stents.

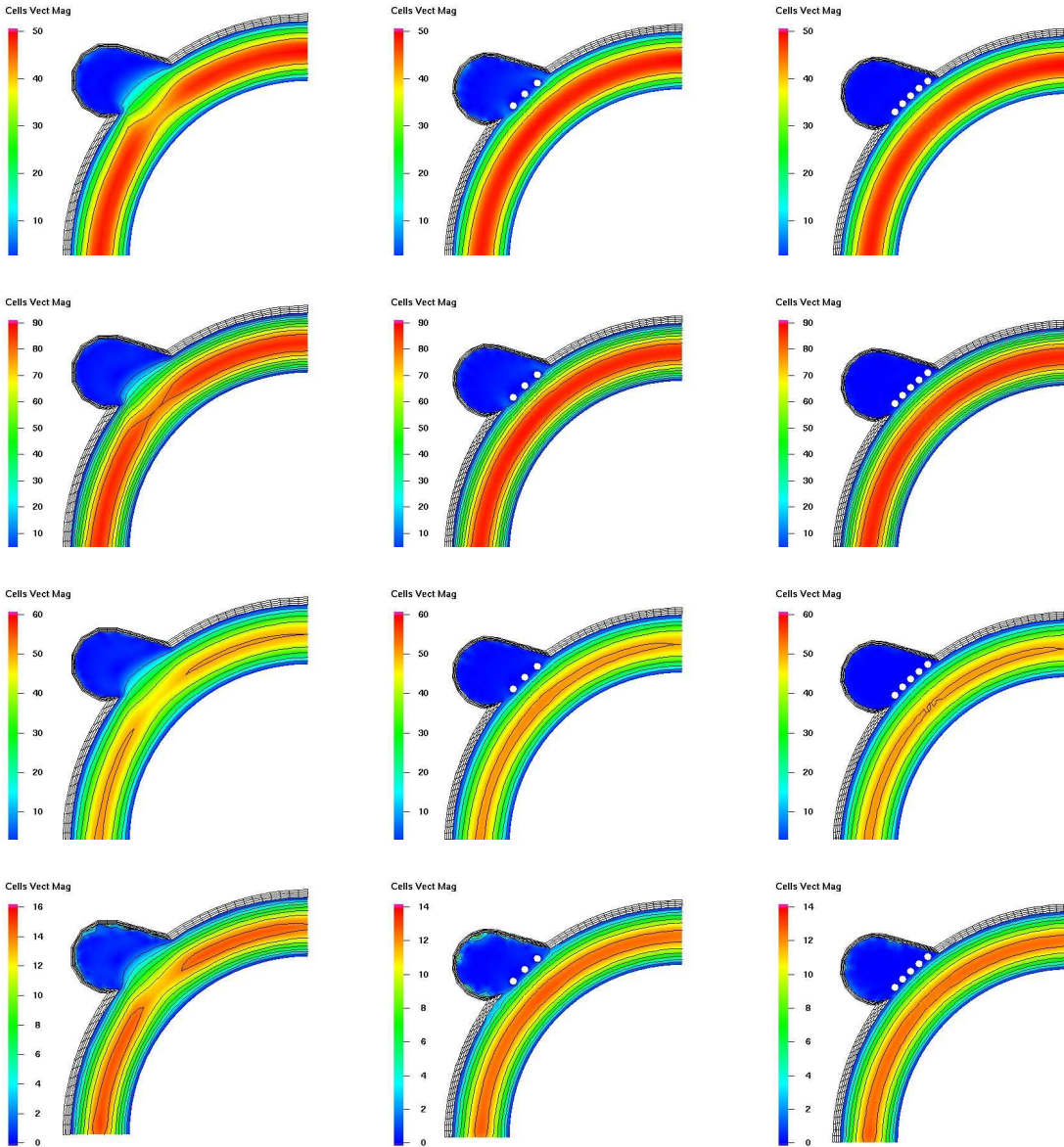


Figure 13: Left column: no stent. Middle column: 3 stents. Right column: 5 stents. Figures demonstrate the global behaviour of the velocity magnitude during one cycle.

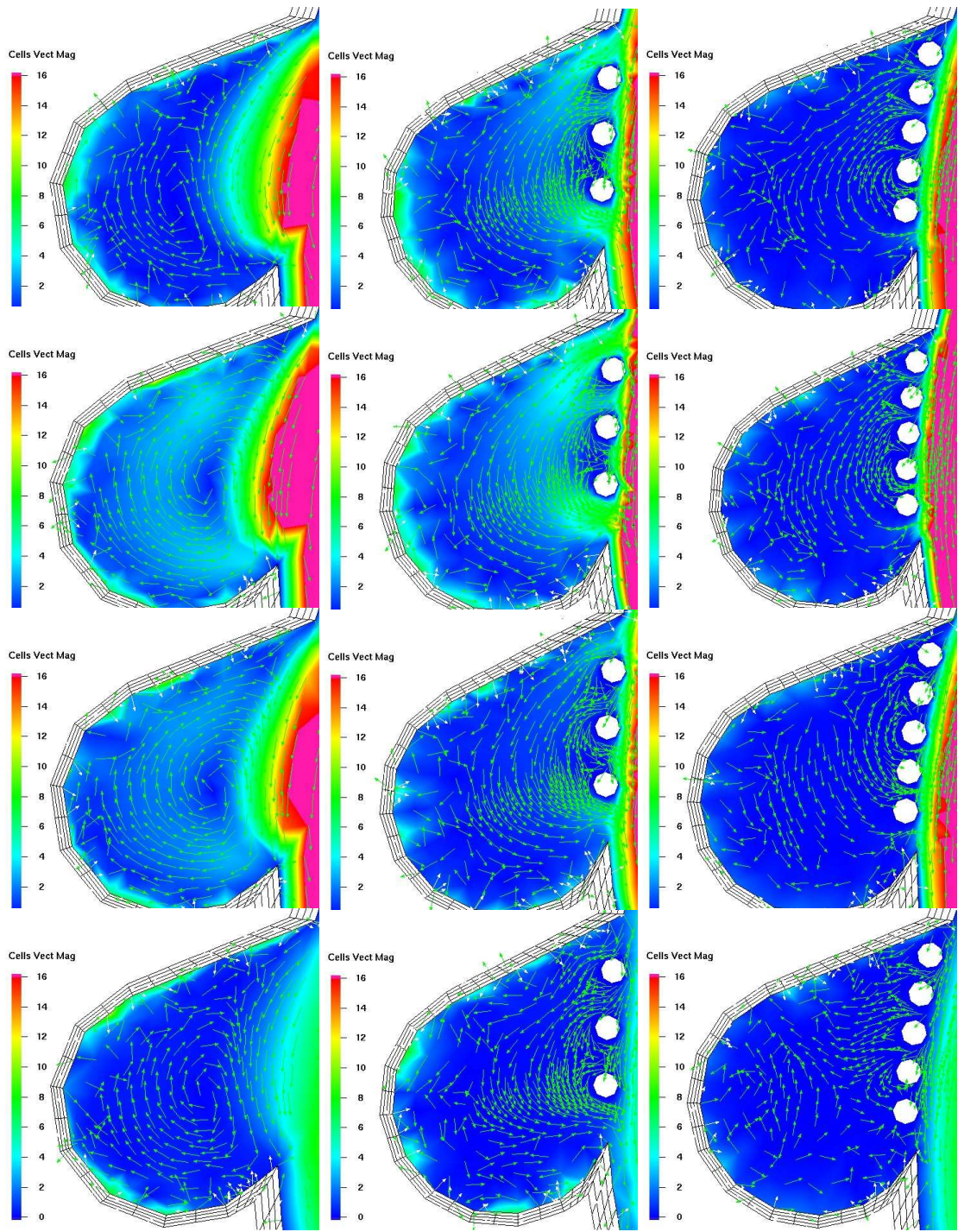


Figure 14: Left column: no stent. Middle column: 3 stents. Right column: 5 stents. Figures demonstrate the local behaviour of the fluid flow inside of the aneurysm during one cycle.

6 Summary and future developments

We presented a monolithic ALE formulation of fluid-structure interaction problems suitable for applications with finite deformations of the structure and laminar viscous flows, particularly arising in biomechanics. The corresponding discrete nonlinear systems result from the finite element discretization by using the high order Q_2P_1 FEM pair which are solved monolithically via discrete Newton iteration and special Krylov-multigrid approaches. While we restricted in the presented studies to the simplified case of newtonian fluids and small deformations, the used numerical components allow the system to be coupled with additional models of chemical and electric activation of the active response of the biological material as well as power law models used to describe the shear thinning property of blood. Further extension to viscoelastic models and coupling with mixture based models for soft tissues together with chemical and electric processes would allow to perform more realistic simulations for real applications.

In this contribution, we applied the presented numerical techniques to fluid-structure interaction problems which examine prototypically the influence of endovascular stent implantation onto aneurysm hemodynamics. The aim was, first of all, to study the influence of the elasticity of the walls onto the flow behaviour inside of the aneurysm. Moreover, different geometrical configurations of implanted stent structures have been analysed in 2D. These 2D results are far from providing quantitative results for such a complex multiphysics configuration, but they allow a qualitative analysis w.r.t. both considered components, namely the elastic behaviour of the structural parts and the multiscale flow behaviour due to the geometrical details of the stents. We believe that such basic studies may help towards the development of future ‘Virtual Flow Laboratories’ which individually assist to develop personal medical tools in an individual style.

Acknowledgment: The authors want to express their gratitude to the German Research Association (DFG), funding the project as part of FOR493 and TRR30, the Jindrich Necas Center for Mathematical Modeling, project LC06052 financed by MSMT, and the Higher Education Commission (HEC) of Pakistan for their financial support of the study. The present material is also based upon work kindly supported by the Homburger Forschungsförderungsprogramm (HOMFOR) 2008.

References

- Appanaboyina, S.; Mut, F.; Löhner, R.; Scrivano, E.; Miranda, C.; Lylyk, P.; Putman, C.; Cebal, J.: Computational modelling of blood flow in side arterial branches after stenting of cerebral aneurysm. *International Journal of Computational Fluid Dynamics*, 22, (2008), 669–676.
- Arnold, D. N.; Boffi, D.; Falk, R. S.: Approximation by quadrilateral finite element. *Math. Comput.*, 71, (2002), 909–922.
- Barrett, R.; Berry, M.; Chan, T. F.; Demmel, J.; Donato, J.; Dongarra, J.; Eijkhout, V.; Pozo, R.; Romine, C.; Van der Vorst, H.: *Templates for the solution of linear systems: Building blocks for iterative methods*. SIAM, Philadelphia (PA 1994).
- Boffi, D.; Gastaldi, L.: On the quadrilateral Q_2P_1 element for the stokes problem. *Int. J. Numer. Meth. Fluids.*, 39, (2002), 1001–1011.
- Bramley, R.; Wang, X.: *SPLIB: A library of iterative methods for sparse linear systems*. Department of Computer Science, Indiana University, Bloomington, IN (1997), <http://www.cs.indiana.edu/ftp/bramley/splib.tar.gz>.
- Damanik, H.; Hron, J.; Ouazzi, A.; Turek, S.: A monolithic FEM approach for non-isothermal incompressible viscous flows. In: *Journal of Computational Physics*, accepted (2008).
- Davis, T. A.; Duff, I. S.: A combined unifrontal/multifrontal method for unsymmetric sparse matrices. *SACM Trans. Math. Software*, 25, (1999), 1–19.
- Fernandez, M. A.; Gerbeau, J.-F.; Martin, V.: Numerical simulation of blood flows through a porous interface. *ESAIM: Mathematical Modelling and Numerical Analysis*, 42, (2008), 961–990.
- Gresho, P. M.: On the theory of semi-implicit projection methods for viscous incompressible flow and its implementation via a finite element method that also introduces a nearly consistent mass matrix, part 1: Theory. *Int. J. Numer. Meth. Fluids.*, 11, (1990), 587–620.

- Hron, J.; Ouazzi, A.; Turek, S.: A computational comparison of two fem solvers for nonlinear incompressible flow. In: E. Bänsch, ed., *Challenges in Scientific Computing*, LNCSE, pages 87–109, Springer (2002).
- Hron, J.; Turek, S.: *Lecture Notes in Computational Science and Engineering, Fluid –Structure Interaction – Modelling, Simulation, Optimization*. Springer, ISBN 3–540–34595–7 (2006a).
- Hron, J.; Turek, S.: A monolithic FEM/multigrid solver for ALE formulation of fluid structure interaction with application in biomechanics. In: H.-J. Bungartz; M. Schäfer, eds., *Fluid-Structure Interaction: Modelling, Simulation, Optimisation*, LNCSE, Springer (2006b).
- Löhner, R.; Cebal, J.; Appanaboyina, S.: Parabolic recovery of boundary gradients. *Communications in Numerical Methods in Engineering*, 24, (2008), 1611–1615.
- Rannacher, R.; Turek, S.: A simple nonconforming quadrilateral stokes element. *Numer. Methods Partial Differential Equations.*, 8, (1992), 97–111.
- Razzaq, M.: *Numerical techniques for solving fluid-structure interaction problems with applications to bio-engineering*. PhD Thesis, TU Dortmund, to appear (2009).
- Razzaq, M.; Hron, J.; Turek, S.: Numerical simulation of laminar incompressible fluid-structure interaction for elastic material with point constraint. In: *Advances in Mathematical Fluid Mechanics-Dedicated to Giovanni Paolo Galdi on the Occasion of his 60th Birthday*, Springer, submitted (2008).
- Tezduyar, T.; Sathe, S.; Cragin, T.; Nanna, B.; Conklin, B.; Pausewang, J.; Schwaab, M.: Modeling of fluid structure interactions with the space time finite elements: Arterial fluid mechanics. *International Journal for Numerical Methods in Fluids*, 54, (2007), 901–922.
- Tezduyar, T.; Sathe, S.; Schwaab, M.; Conklin, B.: Arterial fluid mechanics modeling with the stabilized space time fluid structure interaction technique. *International Journal for Numerical Methods in Fluids*, 57, (2008), 601–629.
- Torri, R.; Oshima, M.; Kobayashi, T.; Takagi, K.; Tezduyar, T.: Influence of wall elasticity in patient-specific hemodynamic simulations. *Computers and Fluids*, 36, (2007a), 160–168.
- Torri, R.; Oshima, M.; Kobayashi, T.; Takagi, K.; Tezduyar, T.: Numerical investigation of the effect of hypertensive blood pressure on cerebral aneurysm dependence of the effect on the aneurysm shape. *International Journal for Numerical Methods in Fluids*, 54, (2007b), 995–1009.
- Turek, S.: *Efficient Solvers for Incompressible Flow Problems: An Algorithmic and Computational Approach*. Springer-Verlag (1999).
- Turek, S.; Rivkind, L.; Hron, J.; Glowinski, R.: Numerical study of a modified time-stepping theta-scheme for incompressible flow simulations. *Journal of Scientific Computing*, 28, (2006), 533–547.
- Turek, S.; Schmachtel, R.: Fully coupled and operator-splitting approaches for natural convection flows in enclosures. *International Journal for Numerical Methods in Fluids*, 40, (2002), 1109–1119.
- Valencia, A.; Ladermann, D.; Rivera, R.; Bravo, E.; Galvez, M.: Blood flow dynamics and fluid–structure interaction in patient -specific bifurcating cerebral aneurysms. *International Journal for Numerical Methods in Fluids*, 58, (2008), 1081–1100.
- Vanka, S.: Implicit multigrid solutions of Navier-Stokes equations in primitive variables. *J. of Comp. Phys.*, 65, (1985), 138–158.

Address: M. Razzaq (corresponding author), S. Turek, and J. F. Acker, Angewandte Mathematik und Numerik, (LS III), TU Dortmund, Vogelpothsweg 87, D-44227, Dortmund, Germany. (mrazzaq@math.tu-dortmund.de)
 J. Hron, Institute of Mathematics, Charles University, Prague, Czech Republic.
 F. Weichert, Department of Computer Graphics, TU Dortmund, Germany.
 I. Q. Grunwald, C. Roth, Department of Neuroradiology, M. Wagner, Department of Pathology, Saar State University Medical School, Homburg Saar, Germany.
 B. F. Romeike, Department of Neuropathology, Friedrich-Schiller University Jena, Germany.